STRATEGIES FOR RAPID TARGET REACQUISITION: PRINCIPLES AND THEORETICAL ADVANTAGES.

Y. Pailhas Ocean Systems Laboratory, School of EPS, Heriot-Watt University, Edinburgh, U.K.
C. Capus Ocean Systems Laboratory, School of EPS, Heriot-Watt University, Edinburgh, U.K.
K. Brown Ocean Systems Laboratory, School of EPS, Heriot-Watt University, Edinburgh, U.K.

1 INTRODUCTION

Much effort has been invested in the processing of sidescan and other imaging sonar data in order to identify and classify targets. Image processing, using for instance Bayesian methods, may classify targets by the intensity, the shape of the target itself or of its shadow. Such methods allow us to process a large amount of data quickly and produce good results - fusion techniques can typically achieve around 90% detection with a 5% false alarm rate, though performance will decline rapidly in heavily cluttered regions. Limits on the information available from processing of intensity imagery are not solely due to the resolution of the acoustic image. To produce more accurate detection and classification new approaches are needed. One method is to send back an AUV in order to reacquire and further inspect a specific target. In this paper we present a strategy for rapid target reacquisition for identification and classification. Building on the physics of ultrasonic wave propagation and scattering and the interaction between acoustic waves and objects, we demonstrate that the analysis of target responses to a broadband signal can give more detailed information on the geometry and material properties of a particular object. Particular target aspects can give a content rich echo ideal for classification and it is crucial that the reacquisition strategy provides a good range of multiview returns. We begin the paper with a brief review of some of the physical theories and models that can be applied to understanding of the echo structure, especially for the case of cylindrical shells. These models explain the principles of resonance for these objects and we review a classification approach based on resonance features. Using this technique, objects with the same target strength and similar shape can be discriminated. The limitations of this approach for different target aspects are examined in section 4 along with new models for finite cylindrical shells backscattering far from the broadside angle. Section 5 discusses the proposed target reacquisition strategy using the multiview aspects and presents some early data from a REMUS autonomous underwater vehicle (AUV) reacquisition trial.

2 THEORETICAL BACKGROUND

In this section we focus our analysis on backscattering from cylindrical shells. Two models are introduced in order to explain briefly the resonance phenomena of these targets.

2.1 Analytical solution

In the case of scattering from an infinite cylindrical shell, an exact solution to the wave equation, including the shear velocity in the solid, can be given[1]. This solution comes from a modal decomposition, and can be well approximated in the case of far field backscattering by:

$$p_s = P_0\sqrt{\frac{2}{\pi kr}}e^{jkr}e^{-j\pi/4}f_\infty e^{j\omega t}$$

The form function f_∞ is given by: $\sum_{n=0}^{+\infty}(-1)^n\varepsilon_n b_b$ is the solution of the system of equations and is determined by the ratio of two 6 x 6 determinants as suggested by Cramer. b_n is a function of the density and the compressional velocity of the two fluids inside and outside the cylinder, the

dimension (a and b outer and inner diameter), the density and the acoustic properties. Note that this result is valid for a monochromatic plane wave. However an extension for any incoming pulse $g_i(t)$ was proposed by Hickling[2]. The frequency representation of the echo $g_s(ka)$ is given by:

$$g_s(ka) = \frac{a}{2r} f_\infty(ka) \int_{-\infty}^{+\infty} p_i(\tau) e^{jka\tau} d\tau$$

with $\tau = (ct - r)/a$. The theoretical echo in the time domain results from inverting this expression through the inverse Fourier transform.

2.2 Models

The analytical solution given in the previous section allows us to analyse the different resonances (Resonance Scattering Theory: RST) through the different modes[3]. This section will present two models explaining the echo structure and the interaction between the incoming wave and the cylinder from a physical point of view. The following assumptions are made: the wall thickness is supposed thin, b/a > 0.95, where b is the inner radius and a is the outer radius; the range of frequencies considered covers 10<ka<50, with k being the wavenumber.

2.2.1 Geometrical Acoustics

We assume for this model that the acoustic impedance between the water and cylinder material is low. This model is valid for materials such as plastics and is drawn from an analogy with geometrical optics. In the case of the cylindrical shell, the first two main echo components are formed predominantly by reflections from the front (specular echo) and the back of the cylinder. The front and back of the cylinder act like spherical mirrors (respectively convex and concave). A numerical simulation done with a Finite Difference Time Domain model[4] allows a 2D visualisation of the interaction between the acoustic wave and a plastic (PVC) shell cylinder (see Figure 1). The two echoes are cylindrical waves and the sources of these waves can be computed. The positions of these sources correspond to the source images computed thanks to the geometrical optics formula for spherical mirrors:

$$\frac{1}{SA'} + \frac{1}{SA} = \frac{2}{SC}$$

where C represents the centre of the sphere, A the source and A' the source image.

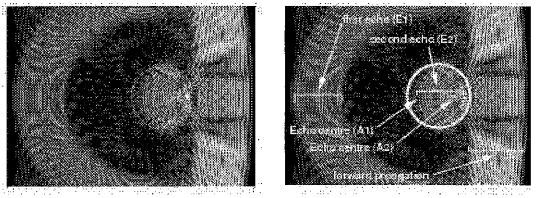

Figure 1 : Visualization of the interaction between the incoming wave and the PVC shelled cylinder. In the annotated diagram the position of the cylinder is indicated by the bold circle.

2.2.2 Geometrical Theory of Diffraction

In this model we assume that the impedance between the water and material is high. This model is valid for materials such as metals. The backscattering from the cylindrical shell can be predicted thanks to a generalisation of the geometrical theory of diffraction (GTD)[5,6]. In this model we consider that the echo is formed predominantly by the specular echo and by the diffracted surface elastic waves. The sound propagation of the plate wave in the cylinder is schematically drawn in Figure 2.

According to the GTD, these plate waves are excited in the shell close to the critical angle θ_c which refers to the relation:

$$\theta_c = \arcsin\left(\frac{c}{c_{plate}}\right)$$

where c_{plate} is the Lamb wave velocity, c the sound speed in water.

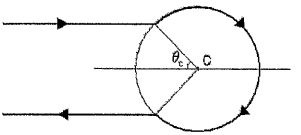

Figure 2 : Propagation of the surface elastic waves on the cylinder in broadside and its backpropagation by diffraction.

So the delay time between the specular echo and the Lamb waves can be evaluated by:

$$\tau = a\left(\frac{1-\cos\theta_c}{c} + \frac{\pi-\theta_c}{c_{plate}}\right)$$

The Lamb velocity can be found by solving the propagation equation in a solid plate[7,8].

3 CLASSIFICATION IN BROADSIDE ASPECT

The previous section explains the formation of echoes in the case of cylindrical shells. According to these models the main echo structure, in a first approximation, will be formed by the specular echo and secondary echoes with a delay between them directly related to the dimension of the object.
In the Fourier domain the integration of this structure creates strong oscillations in the range of frequencies we are considering. These oscillations correspond to the resonances of the object. For simple man-made objects (i.e. simple smooth shape) we can assume the previous models are valid and the echo spectra are strongly influenced by the resonances. Taking into account these hypotheses, it appears relevant to consider the location of the notches and peaks in the echo spectra as strong features for identification.

Experiments have been done in the wave-tank at Heriot-Watt University. Insonifying different objects with the bio-inspired pulses described in[9], the echoes of 5 different objects have been analysed[10]. Features are extracted by applying a threshold to output a binary spectral signature for the target. Eleven echoes have been recorded for each pulse/target combination investigated, with the sonar head scanning across the target in the range -10° to +10° in 2° steps. The resultant spectral bar-codes are stacked into a binary image containing all bar-code responses for that target. Figure 3 shows eight "bar-code" images for a range of targets under test. For each target (apart from the tank floor) the binary responses are very consistent between pulses and sonar head angle. This observation confirms that these features are stable under these test conditions.

From the binary representations it is possible to compute a confusion matrix in order to see the classification properties of the features. The confusion matrix displayed in Figure 3 uses the Manhattan distance $\sum_{i,j}\left|x_i - y_j\right|$ and compares one target echo to all the other responses for each target. The matrix is highly diagonal indicating a high degree of classification potential using these features. Looking at the cross correlation, a few points are particularly interesting in our discussion. First we note similarities between the steel pipe and the PVC tube. Indeed both are cylindrical shells with almost the same outer diameter (only 3mm differences between them). Because of these properties we are encouraged to see some correlation between them. In terms of target strength, there is only 1.6dB difference at 100 kHz between the two cylinders. However using the spectral features permits an reliable classification. The second point of interest is the strong

correlation between cone 1 and cone 2. Both represent the same cone-like target but with a tilt of 8° between 1 and 2. This demonstrates some consistency in response for a range of angles of view close to broadside. The brick 1 and brick 2 responses, which represent the same object but with a relative rotation of 90°, show a poor cross correlation.

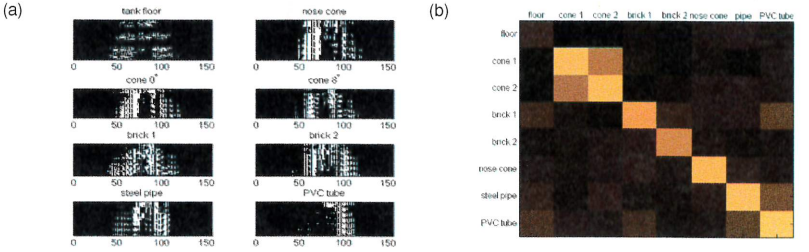

Figure 3 : *(a)* Spectral bar-code for seven bottom-set targets. 66 responses are encoded for each target corresponding to the six transmit pulses and eleven head angles used. The horizontal scale is frequency in kHz. *(b)* Confusion matrix.

4 MULTIVIEW ASPECT

To further explore aspect limitations on classification from characteristic spectral responses, we now focus our attention on multi-aspect returns from finite cylindrical shells. Several studies have been done on backscattering from these targets[11,12]. The aim is to determine limitations on the detection of the resonances described earlier. We also propose a simple model for the backscattered echo for angles far from the broadside aspect.

4.1 Theoretical limitation in broadside

We consider a finite cylinder (length = L) insonified by a sonar at a distance r. We suppose that the sonar is far enough away to ensure that receive and transmit beam-patterns cover the entire cylinder. In this case, the limit angle θ_{lim} depends only on the parameters L and r and is given by the formula:

$$\theta_{\text{lim}} = \arcsin\frac{L}{2r}$$

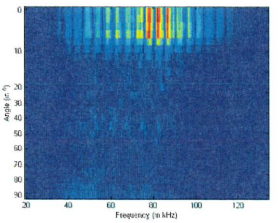

Figure 4 : Spectra of the backscattering echo of a PVC tube (0.8m long in function of the angle of incidence)

Below θ_{lim} we expect the same peaks and notches in the echo spectra as in the broadside view described earlier. This result is confirmed by experimentation done with a finite 110mm diameter PVC tube in the test tank. In this case L = 80cm and r = 2.6m, giving strong features up to $\theta_{lim} \approx 9^{\circ}$ which is confirmed by Figure 4.

4.2 The bistatic approach

In this case the cylinder is centred at the origin; the transmitter is on the 0° axis. The cylinder is rotated by an angle θ in the horizontal plane. Above the limit angle θ_{lim}, the main energy of the echo will be transmitted at an angle of 2θ. In line with section 2.2, we consider the two approaches given. The delay between the specular echo and the reflected or diffracted second echo Δt is calculated at the 2θ axis. In these equations: a is the diameter of the cylinder, c the sound speed in water, and c_{plate} the Lamb wave velocity. In the geometrical acoustic case, the sound propagation is illustrated in Figure 5 (a). The resonances will be dominated by Δt given by:

$$\Delta t = \frac{2a}{c}\cos\theta$$

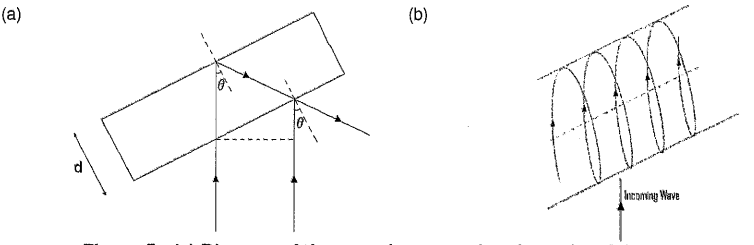

Figure 5 : (a) Diagram of the sound propagation through a finite cylindrical shell with an angle θ following the model of geometrical acoustic; *(b)* Propagation of the surface elastic waves on a finite cylindrical shell insonified with an angle θ. This diagram corresponds to the GTD case.

In the GTD case, the resonances come from the diffraction of the plate waves propagating on the surface of the cylinder. Because of the angle of incidence θ, the trajectory of these plate waves will be a helix as drawn in Figure 5 (b). The resonances will be dominated by Δt given in the next equation:

$$\Delta t = \frac{2a}{c_{plate}}\sqrt{1+\tan^2\theta\sin^2\gamma}\,\sin(\sin\gamma) \text{ with } \gamma = \arctan\frac{\cos\theta}{\cos\theta_c}.$$

This suggests that with a receiver in this axis, the characteristic resonances of the cylinder could still be observed.

4.3 Model for angle far from broadside in the time domain

A simple model for angles higher than the limit angle is to consider only the diffraction by four edges of the cylinder, see Figure 6 (a). This simplification allows us to match the echo time structure, Figure 6 (b), with the point diffraction model, Figure 6 (c).

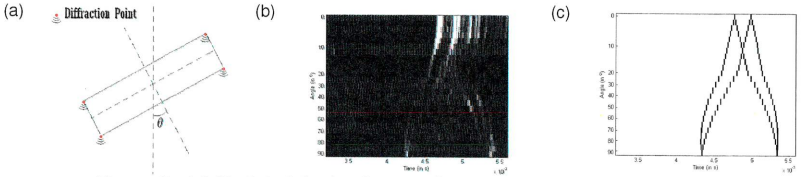

Figure 6 : (a) Model of the backscattering contribution of the diffraction of the 4 edges of the cylinder. Display of the echo structure of the PVC tube in the time domain: *(b)* experiment data, *(c)* model.

Figure 7 gives a little more detail for the echo structure of the PVC tube in the time domain. Depending on the angle of view, different physical processes are seen to contribute to the echo formation. Close to the broadside angle we find strong resonances as discussed in section 3. Far from the broadside angle it is principally the diffraction phenomenon which is dominant.

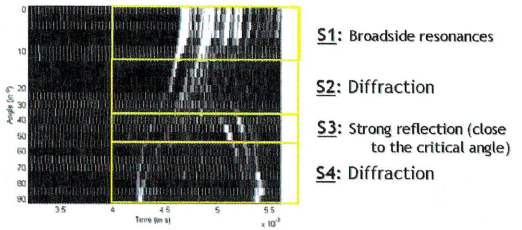

Figure 7 : Visualisation of the different physical phenomena in the composition of the echo depending of the angle of view.

4.4 Acoustical tomographic reconstruction

Considering the previous point diffraction model, it is possible to reconstruct an image of the density of reflectivity of the target thanks to tomographic techniques. Indeed let f(x,y) be the density of reflectivity, $p_r(t,\theta)$ the intensity of the echo. We denote $S_\theta(\omega) = TF[\, p_r(t,\theta)\,]$. One can show that the reconstruction of the reflectivity image $\hat{f}(x,y)$ can be obtained with the equation:

$$\hat{f}(x,y) = \int_0^{2\pi} \int_{-\infty}^{+\infty} S_\theta(\omega) e^{j\omega x} d\omega d\theta$$

Figure 8 shows an example of tomographic reconstruction for a complex target: a large convex open-ended cone. The cone was insonified at various angles (on a 180° sector with 5° interval). The reconstructed image shows the main diffraction points of the cone and the acoustic focus points.

(a) (b)

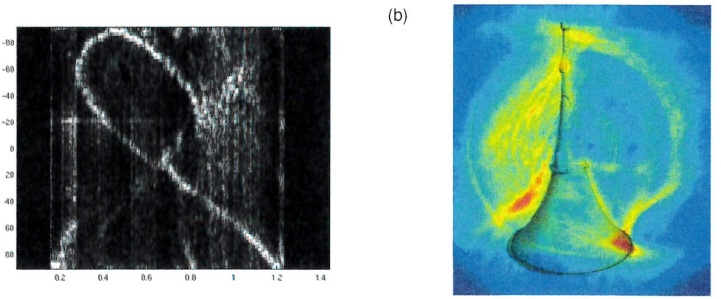

Figure 8 : (a) Display of the echo structure of the cone in the time domain through the angles -π/2 to π/2. *(b)* tomographic reconstruction.

5 REACQUISITION STRATEGY

A standard AUV reacquisition strategy consists of the survey of the target with three different angles. At most, six different aspects of the target are available. Note that for each target inspection the AUV may run for more than 1000m. To gain full value from multiaspect data, the proposed revised strategy consists of running a circular trajectory around the target. In the ideal case a continuous multiview of the target is available. So, using broadband sonar, resonances can be extracted from returns near the broadside aspect and robust classification (cf. section 3) can be achieved. A further important gain is in terms of time. For a 20m diameter circle and a survey of three turns, the AUV runs only 190m.

(a) (b)

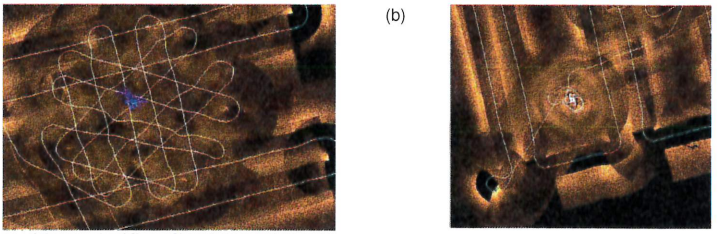

Figure 9 : Visualization of the techniques of reacquisition of target, superposition of the sidescan images and the trajectory of REMUS (in white) *(a)* traditional, *(b)* new circular strategy.

Experiments have been done in Loch Earn, Scotland, using the REMUS AUV. Missions for specific target reacquisitions have been run using the circular trajectory. In these early trials only sidescan data were available. In reproducing images of a wreck on the Loch bed, Figure 10 demonstrates that good mosaicing and reconstruction results can be achieved using the non-standard circular reacquisition strategy with a conventional sensor.

6 CONCLUSION

This paper has presented a revised strategy for target reacquisition suitable for AUV operations. This technique has two major advantages: first it is much quicker than the traditional one, and second it gives access to a continuous multiview aspect of the target. The latter is useful for gaining full value from wideband spectral features which provide highly discriminatory target information over a limited range of aspect angles. In the case of cylindrical shells, theoretical limitations have

been derived and shown to match well with experimental results. We have shown that tomographic reconstruction is possible given a sufficient number of multiaspect views of the target and that results can be related to the underlying physical scattering processes. Data gathered in real world trials at Loch Earn have also shown that good results can still be generated from conventional imaging sonar data using the circular reacquisition profile.

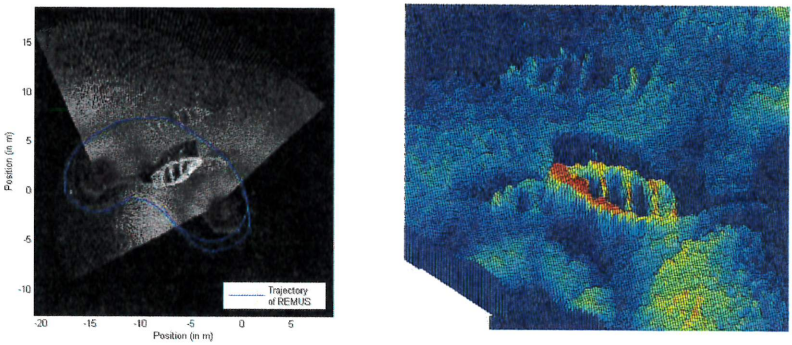

Figure 10 : Target (wreck) reconstruction by registration of sidescan pings from the revised reacquisition profile

7 REFERENCES

1. R.D. Doolittle and H. Uberall, Sound Scattering by Elastic Cylindrical Shells, J. Acoust. Soc. Am. 39(2), 272-275 (1966).
2. R. Hickling, Analysis of Echoes from a Solid Elastic Spher in Water, J. Acoust. Soc. Am. 34, 1582-1592 (1962).
3. G.C. Gaunaurd and H. Uberall, RST analysis of monostatic and bistatic acoustic echoes from an elastic sphere, J. Acoust. Soc. Am. 83, 25-37 (1988).
4. M. Lianantonakis and J. Bell, Sonar Simulation: Modelling the effect of shear from elastic objects and seabeds, Internal Report (2003).
5. P.L. Marston, GTD for backscattering from elastic spheres and cylinders in water and coupling of surface elastic waves with the acoustic field, J. Acoust. Soc. Am. 83, 25-37 (1988).
6. S.G. Kargl and P.L. Marston, Observations and modelling of the backscattering of short tone bursts from spherical shell: Lamb waves echoes, glory, and axial reverberation, J. Acoust. Soc. Am. 85(3), 1014-1028 (1989).
7. H. Lamb, On waves in an elastic plate, Proc. R. Soc. London Ser. 93, 114-128 (1917).
8. T.N. Grigsby and E.J. Tajchman, Properties of Lamb: Waves Revelant to the Ultrasonic Inspection of Thin Plates, IRE Trans. Ultrason. Eng UE-8, 26-33 (1961).
9. C. Capus, Y. pailhas, K.E. Brown, D.M. Lane, P. Moore and D. Houser, Bio –inspired wideband sonar signals based on observation of the bottlenose dolphin (Tursiops Truncatus), J. Acoust. Soc. Am. 121(1), 594-604 (2007).
10. C. Capus, Y. Pailhas and K.E. Brown, Classification of bottom-set targets from wideband echo responses to bio-inspired sonar pulses, Institute of Acoustics, 4th International Conference on Bioacoustics, Loughborough, UK, April 2007.
11. X-L. Bao, Echoes and helical surface waves on finite elastic cylinder excited by sound pulses in water, J. Acoust. Soc. Am. 94, 1461-1466 (1993).
12. S.F. Morse and P.L. Marston, Backscattering of transient by tiltes truncated cylindrical shells: Time-frequency identification of ray contributions from measurements, J. Acoust. Soc. Am. 111(3). 1289-1294 (2002).